J. Fluid Mech. (1985), *vol.* 159, *pp.* 85–104
Printed in Great Britain

An experimental study of organized motions in the turbulent plane mixing layer

By A. K. M. F. HUSSAIN AND K. B. M. Q. ZAMAN†
Department of Mechanical Engineering, University of Houston, Houston, Texas 77004

(Received 25 July 1984 and in revised form 12 March 1985)

Large-scale coherent structures in a large, single-stream plane mixing layer of air have been investigated experimentally. The *unforced, initially fully turbulent* mixing layer rolls up into organized structures whose average passage frequency f_m at any downstream distance x from the lip depends on x. These structures are detected for the entire length of the measurement, i.e. up to $x = 3$ m or $5000\theta_e$. The Strouhal number St_θ ($= f_m \theta / U_e$) is observed to be a constant (≈ 0.024) at all x. θ_e and θ are, respectively, the exit and local momentum thicknesses of the mixing layer, and U_e is the free-stream velocity. (The entrainment velocity on the zero-speed side is found to be $0.032U_e$.) The coherent-structure properties are educed in the developing and self-preserving regions of the mixing layer using an optimized conditional-sampling method, triggered on the peaks of a local reference $\tilde{u}$-signal obtained from the high-speed edge of the layer. Sectional-plane contours of the properties of the structure such as coherent vorticity, Reynolds stress and production reveal that the structure formation and evolution are complete by $x \cong 500\theta_e$, beyond which the structure achieves an 'equilibrium' state as defined by the structure properties.

1. Introduction

Recent investigations continue to suggest that turbulent shear flows are generally characterized by large-scale coherent structures (Brown & Roshko 1974; Townsend 1979; Roshko 1980). There is strong evidence that such structures occur not only in the near fields (Crow & Champagne 1971), but also in the self-preserving regions (Tso 1983) of axisymmetric jets. Coherent structures presumably also occur in fully turbulent wakes (Grant 1958; Keffer 1965; Cimbala 1984), plane jets (Mumford 1982; Moallemi & Goldschmidt 1981), and boundary layers (Brown & Thomas 1977; Head & Bandyopadhyay 1981). Little is known, however, about the detailed characteristics and dynamical roles of these structures, even in the simplest turbulent shear flow, namely the plane mixing layer.

Browand & Weidman (1976) obtained vorticity contours and Reynolds-stress variations for a stage of pairing of the structures; but they did this in a very low-Reynolds-number two-stream plane mixing layer, which was considered by others (e.g. Yule 1978) as non-representative of large-Reynolds-number (i.e. asymptotic) mixing layers. From autocorrelation measurements of longitudinal velocity signals as well as flow visualization, Dimotakis & Brown (1976) deduced the existence of large-scale structures in an initially laminar, high-Reynolds-number, two-stream mixing layer. However, they did not attempt to educe the structure properties or address their dynamical role. In fact, much needs to be done to explore the detailed

† Current address: NASA Langley Research Center, M.S. 359, Hampton, VA 23665.

topological properties and to understand the dynamics of the coherent structures in the self-preserving region of any shear flow.

The motivation for the present study stemmed from a number of outstanding questions. Does a natural (i.e. unexcited), initially fully turbulent mixing layer roll up into organized structures? If so, how do the structures evolve in this flow? Do these structures occur in the asymptotic region of the flow? If there is an 'equilibrium structure' in the asymptotic state, what are its characteristics? Is there an optimum conditional-sampling criterion for the eduction of these structures? What are the relative contributions of coherent and incoherent turbulence to Reynolds stress and production in the developing and self-preserving regions of the mixing layer?

In what follows, we report the eduction procedure, topological characteristics and mechanics of the large-scale structures in a high-Reynolds-number plane mixing layer, originating from an *initially fully turbulent boundary layer*. For the eduction scheme, we have utilized our experience from a previous study in high-Reynolds-number (unexcited) axisymmetric mixing layers, where a comparative evaluation of alternative sampling criteria was carried out (Zaman & Hussain 1984, *hereinafter referred to as* ZH). Such a comparative evaluation was also carried out in the present flow, the principal outcomes of which will be discussed in §3.2. The differences between the plane and the axisymmetric mixing layers in this connection and regarding the large-scale structure characteristics will be discussed whenever appropriate. The details of the large-scale structures educed in the present study, should be important not only in understanding the physics of shear-flow turbulence but also in the formulation of a viable turbulence theory which must directly incorporate the structures. The results in this paper were presented by the authors at the 1981 APS meeting (Hussain & Zaman 1981*b*) and in detail in a laboratory report (Hussain & Zaman 1982).

2. Experimental apparatus

The experiments were carried out in a large plane mixing layer formed in a 9 m × 4 m × 3.5 m room from which air was sucked out by a blower. Figure 1 gives a schematic diagram of the room. Air circulated back into the room from an adjacent large hall via honeycombs and screens and a contraction terminating into a 48 cm × 96 cm rectangular hole whose three sides were continued downstream into uninterrupted confining walls. The fourth (vertical) side ended in a backward-facing step, whence the mixing layer of 96 cm span was initiated. The free plane mixing layer continued for a streamwise distance of 8 m. However, because of the influences of the boundary layers on the upper and lower confining walls and the opposite parallel wall, and from consideration of the aspect ratio of the mixing layer, the useful length of the mixing layer was about 4 m.

The entrainment air was supplied through a 1.5 m high filter box extending the entire 9 m length of the room. Care was taken to check that the entrainment air supply was uniform and that there was no large-scale circulation within the room. The leading edges of the confining walls were rounded in order to prevent separation of the entrainment-induced boundary layers (figure 1).

At 10 cm upstream of the separation lip, the boundary layer on the nozzle wall was tripped by the serrated edge of a fine-toothed chainsaw blade. This resulted in a fully turbulent state of the mixing layer at the initiation point of the layer, i.e. at the lip (details are discussed in §3.1). We emphasize that three-dimensionality of the trip is important in achieving rapid transition and evolution of the boundary layer.

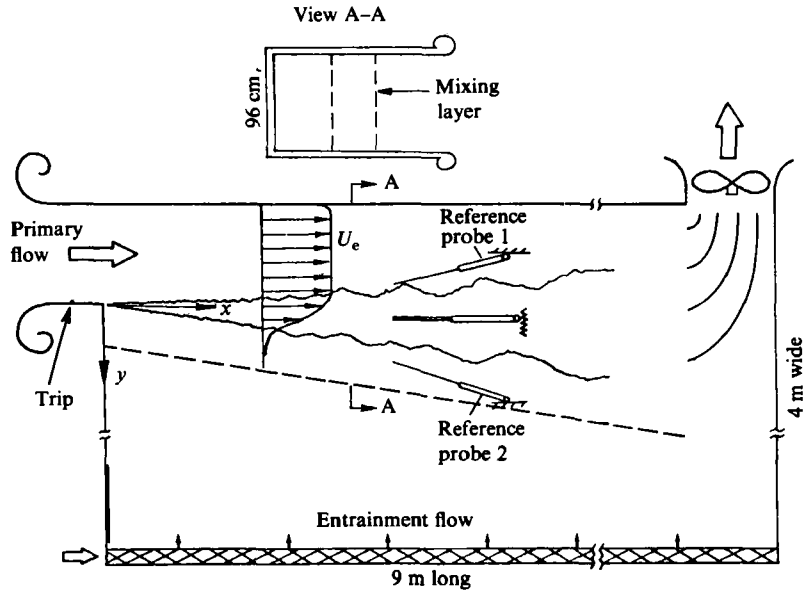

FIGURE 1. Schematic of the flow facility; flow conditions: $U_e = 12$ m s^{-1}; $\theta_e = 0.053$ cm; $R_\theta = 428$.

Results are presented for a free-stream velocity U_e of 12 m s^{-1}. The mean velocity distribution over the cross-section of the entrance hole was found to be uniform to within 2 %. The free-stream turbulence intensity was less than 0.2 %. The exit mean- and fluctuating-velocity profile details were found to be uniform in the spanwise direction for 95 % of the span.

Data were obtained using standard linearized hot-wire (DISA) anemometers. Data acquisition and probe traverses were accomplished via automated computer control. Hot-wire signals were first digitized by a 12 bit A/D converter, stored on a digital magnetic tape and later processed on the laboratory computer (HP2100S). Spectra were obtained on-line with a Spectrascope SD335 spectrum analyser. Further details of the measurements are given in §3.2.

3. Results and discussion

3.1. *Initial condition*

The dependence of free shear flows on the initial condition has been well established (Bradshaw 1966; Batt 1975; Foss 1977). The dependence is typically traceable to the initial instability. Since the flow environment abounds with disturbances from a variety of sources, a natural shear layer is seldom disturbance free (Hussain 1980). The effect of these background disturbances, which appear as 'free-stream turbulence', is typically very prominent in an initially laminar shear layer if the disturbance frequencies fall within the unstable bandwidth of the layer. This effect is less in an initially fully turbulent shear layer unless the disturbances are sufficiently strong in comparison with the turbulence intensity in the layer. Small-amplitude excitations, which produce profound effects on the evolution of an initially laminar shear layer, were found by us to be ineffective in altering the evolution of a fully developed initially turbulent shear layer. (The reason may be both three-dimensionality and

nonlinearity of the fluctuations in the turbulent exit boundary layer.) However, high-amplitude, two-dimensional excitation should be successful in organizing the instability and roll-up of an initially turbulent shear layer. Because a disturbance-free laminar initial condition is hard to achieve and an initially turbulent shear layer is relatively insensitive to free-stream turbulence, the turbulent initial condition was chosen for the present study.

Figures 2(*a–c*) document the fully turbulent state of the exit boundary layer measured just downstream ($x < 1$ mm) from the separation point. Figure 2(*a*) shows the profiles of the longitudinal mean and fluctuation r.m.s. velocities as functions of the distance from the wall, non-dimensionalized by the displacement thickness δ_1. Both the profiles are typical of the turbulent flat-plate boundary layer. The momentum thickness θ_e, the shape factor δ_1/θ_e and the Reynolds number R_θ of the exit boundary layer were 0.053 cm, 1.6 and 428 respectively. The mean-velocity distribution in universal (u^+, y^+) coordinates, shown in figure 2(*b*), exhibits the characteristic logarithmic and wake regions of a turbulent boundary layer. The friction velocity U_τ was determined by the Clauser cross-plot technique. The data show excellent agreement over the logarithmic region with the equilibrium flat-plate equation $u^+ = 5.6 \log y^+ + 4.9$ shown as a straight line in the figure; here $u^+ = U/U_\tau$ and $y^+ = yU_\tau/\nu$. The shape factor, the peak turbulence intensity ($u'/U_\tau \approx 2.4$) and the distance from the wall ($y^+ \approx 20$) where the peak turbulence intensity occurs, the extent of the logarithmic region, etc. agree very well with the data of Purtell, Klebanoff & Buckley (1981) for the corresponding value of R_θ. The wake strength also agrees well with that expected of an equilibrium flat-plate boundary layer (Coles 1962). These data should be adequate to prove that the boundary layer before separation was fully developed turbulent. As a further support, frequency spectra of the $\tilde{u}$-signal at transverse points where the mean velocity equals 99, 50 and 10% of the free-stream mean velocity are shown in figure 2(*c*). In each trace the spectral strength decreases monotonically with increasing frequency and there is no peak or hump. If there were any periodic surging or significant acoustic disturbance, then the spectra, at least the one at $U/U_e = 0.99$, would have revealed it. Therefore any downstream organization of the mixing layer, revealed by distinct humps in the corresponding spectra (see later), must be due to natural evolution of coherent structures alone.

3.2. *Eduction scheme*

The conditional-sampling measurements were made by tape recording velocity signals and subsequent off-line analysis. Four simultaneous velocity signals: two ($\tilde{u}$, $\tilde{v}$) from a measuring X-wire probe, and two from fixed reference probes (figure 1) – one ($\tilde{u}_{r1}$) from the high-speed edge and the other ($\tilde{u}_{r2}$) from the zero-speed edge of the mixing layer – were stored on a digital magnetic tape; u and v denote streamwise and transverse velocity fluctuations respectively. Typical time traces of $\tilde{u}_{r1}$, $\tilde{u}_{r2}$, $\tilde{u}$ and $\tilde{v}$ are shown in figure 3 for $x = 600\theta_e$, where the flow has achieved self-preservation on the basis of all time-average measures (S. J. Kleis, private communication). Note that the signals ($\tilde{u}_{r1}$, $\tilde{u}_{r2}$) from the high- and zero-speed edges of the layer indicate the passage of quasiperiodic structures, the 'footprint' being clearer and stronger on the high-speed edge. Inside the mixing layer, the 'footprint' is buried under high-level turbulence, as is evident from the $\tilde{u}$- and $\tilde{v}$-traces obtained from the $U/U_e \approx 0.65$ point. The sharp spikes in $\tilde{u}$ and $\tilde{v}$, inside the mixing layer, are associated with internal shear fronts and smaller scales, which occur randomly with respect to the structure boundary and thus are unsuitable for use as triggers in the eduction of the coherent structures.

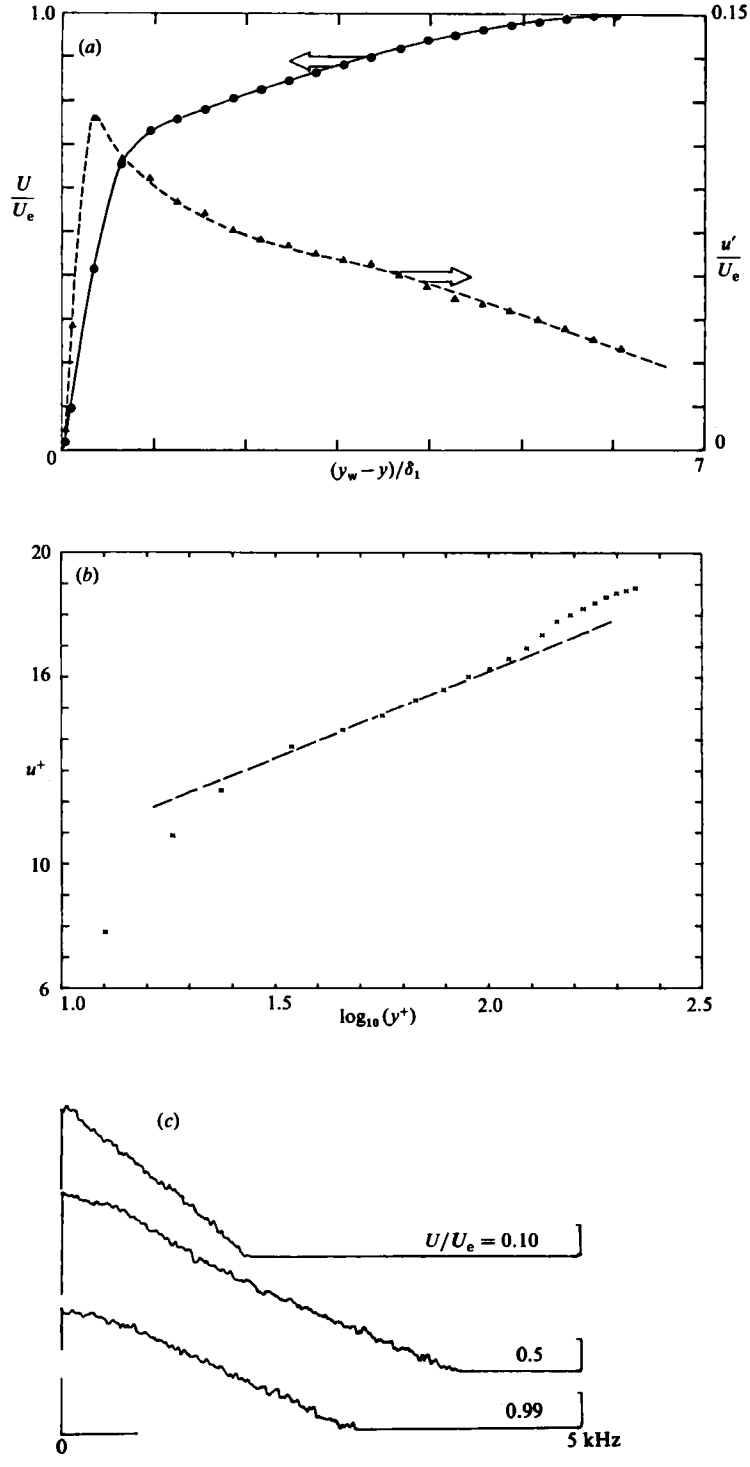

FIGURE 2. Initial conditions: (*a*) mean (U) and r.m.s. (u') velocity profiles at the lip; (*b*) U-profile in (u^+, y^+)-coordinates; (*c*) $\tilde{u}$-spectrum at the lip for three transverse locations.

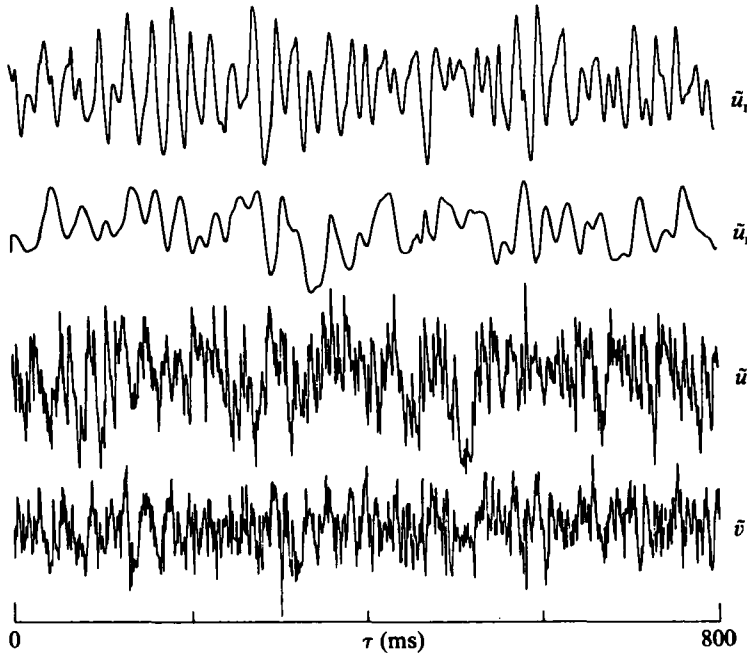

FIGURE 3. Velocity signals at $x/\theta_e = 600$ in the sequence (from top): $\tilde{u}_{r1}$ from the $U/U_e \approx 0.99$ point; $\tilde{u}_{r2}$ from the $U/U_e \approx 0.03$ point; $\tilde{u}$- and $\tilde{v}$-signals from the $U/U_e \approx 0.65$ point.

In the present eduction scheme, the large positive peaks of $\tilde{u}_{r1}$ were used as triggers (discussion of this choice follows). Starting from each trigger, simultaneous $\tilde{u}$- and $\tilde{v}$-signals were sampled (64 points each). Thus ensembles of $\tilde{u}$ and $\tilde{v}$, centred with respect to a trigger, were obtained for each y-station. Averages of these, for 13 y-stations, gave the $\langle u \rangle (t, y)$ and $\langle v \rangle (t, y)$ distributions. The spanwise component Ω_z of the coherent vorticity was then computed using the relation

$$\Omega_z(t, y) = -\frac{1}{0.5U_e}\frac{\partial \langle v \rangle}{\partial t} - \frac{\partial \langle u \rangle}{\partial y}.$$

(For a discussion of the use of the Taylor hypothesis in coherent structures see Zaman & Hussain (1981).) The following decomposition of each instantaneous variable $\tilde{f}$ was used for data analysis:

$$\tilde{f} = \langle f \rangle + f_r, \quad \langle f \rangle = F + \langle f_p \rangle,$$

where F is the time average of $\tilde{f}$, $\langle f_p \rangle$ is the departure of the phase average from F, and f_r is the random, incoherent part (for further details see Hussain & Zaman 1980, *hereinafter referred to as* HZ1).

Conditional-sampling measurements being inherently subjective, care is needed in the choice of the sampling criteria and in the interpretation of the results obtained thereby. A comparative study of the choice of different features of $\tilde{u}_{r1}$ and $\tilde{u}_{r2}$ as triggering criteria was carried out previously in *an axisymmetric mixing layer* by ZH. Contours of Ω_z computed from the same data set by using different triggering criteria were examined. The following triggering criteria were considered: (i) using the peaks of a reference signal discriminated by different threshold levels; (ii) using a window at the threshold level; (iii) triggering on the positive or negative peaks of $\tilde{u}_{r1}$, $\tilde{u}_{r2}$ or a reference $\tilde{v}_r$-signal; (iv) using joint criteria based on simultaneous occurrences of

positive (or negative) peaks in $\tilde{u}_{r1}$ and $\tilde{u}_{r2}$ at selected phase differences and different transverse locations of the reference probes, etc. Contours of Ω_z obtained by the different criteria were compared with one another and with the corresponding contours obtained in the same flow (axisymmetric mixing layer) but with artificial excitation at the 'preferred mode'. Eduction criteria producing sharper structure features with higher core vorticity, which indicates lesser smearing in the eduction, were considered superior. It was found that the simple criterion of triggering on the large positive peaks (above twice the standard deviation) of the a.c. coupled $\tilde{u}_{r1}$ signal, obtained from the high-speed edge of the mixing layer (where $U/U_e \approx 0.99$), was the optimum choice for the eduction. Stricter criteria, requiring longer experiment times, resulted in insignificant improvement in the eduction.

A similar comparative study established that the above optimum eduction criterion applied to the plane mixing layer also. This evaluation was carried out at the axial station $x = 600\theta_e$. A noticeable difference between the axisymmetric and plane mixing layers was that the high- and low-speed side motions in the latter were better correlated. The transverse variations of auto- and cross-correlations $\overline{uu}(\tau)$, $\overline{vv}(\tau)$ and $\overline{uv}(\tau)$ for $x = 600\theta_e$ are first documented as contour maps in figures 4(*a*, *b*, *c*) respectively. For direct comparison of the relative amplitudes, all these quantities have been non-dimensionalized by U_e^2. Note the symmetry of $\overline{uu}$ and $\overline{vv}$ contours in τ, as expected; the antisymmetry of the $\overline{uv}$ contours on the high- and zero-speed sides is consistent with the fact that $\tilde{u}$- and $\tilde{v}$-fluctuations on the outer edges of the mixing layer are mostly potential fluctuations and are thus in quadrature.

The three contours in figures 4(*a*–*c*) are globally quite similar to those in the axisymmetric mixing layer (see ZH). But comparison shows that the quasiperiodicity in the plane mixing layer is detectable over a larger transverse extent. For example, the quasiperiodicity in $\overline{vv}(\tau)$ persists up to $U/U_e \approx 0.3$ (figure 4*b*) as compared with $U/U_e \approx 0.6$ in the axisymmetric case. The higher cross-correlation between the high- and low-speed side motions of the plane mixing layer is clearly demonstrated in figure 4(*d*). It shows the contours of the cross-correlation coefficient between $\tilde{u}_{r1}$ (obtained from the high-speed edge where $U/U_e \approx 0.99$) and the $\tilde{u}$-signal from a probe moved to different y-locations. Note that substantial cross-correlation persists all across the mixing layer. In the axisymmetric case this cross-correlation was found to be essentially zero in the middle of the layer, and the magnitude did not exceed 0.1 anywhere on the zero-speed side. Thus the transverse coherence across the plane mixing layer is stronger than that in the axisymmetric configuration. In the axisymmetric case the high-speed side 'footprint' is accentuated because the induced velocities in the core flow are much stronger than those in the outer, zero-speed side; however, a weaker 'footprint' of the structures on the zero-speed side results in weaker transverse coherence. Furthermore, the flow geometry is believed to augment tearing and fractional and partial pairings in the axisymmetric configuration (Hussain & Clark 1981), contributing to the weaker correlation in the transverse direction.

In view of the foregoing, in contrast with the axisymmetric case (ZH), structure eduction triggered on the peaks of $\tilde{u}_{r2}$ was fairly successful in the plane mixing layer. However, this was not as successful as that based on $\tilde{u}_{r1}$ peaks; this appears to be partly due to inherent hot-wire errors on the zero-speed side, e.g. effects of large fluctuation intensities and hot-wire rectification of $\tilde{u}_{r2}$ during instants of flow reversal (Antonia, Chambers & Hussain 1980; HZ1). Our efforts to capture two structures in any phase of pairing by using joint criteria based on prescribed phase lags between the peaks of $\tilde{u}_{r1}$ and $\tilde{u}_{r2}$ did not succeed. Note that Browand & Weidman (1976) successfully employed this technique in a low-Reynolds-number, two-stream mixing

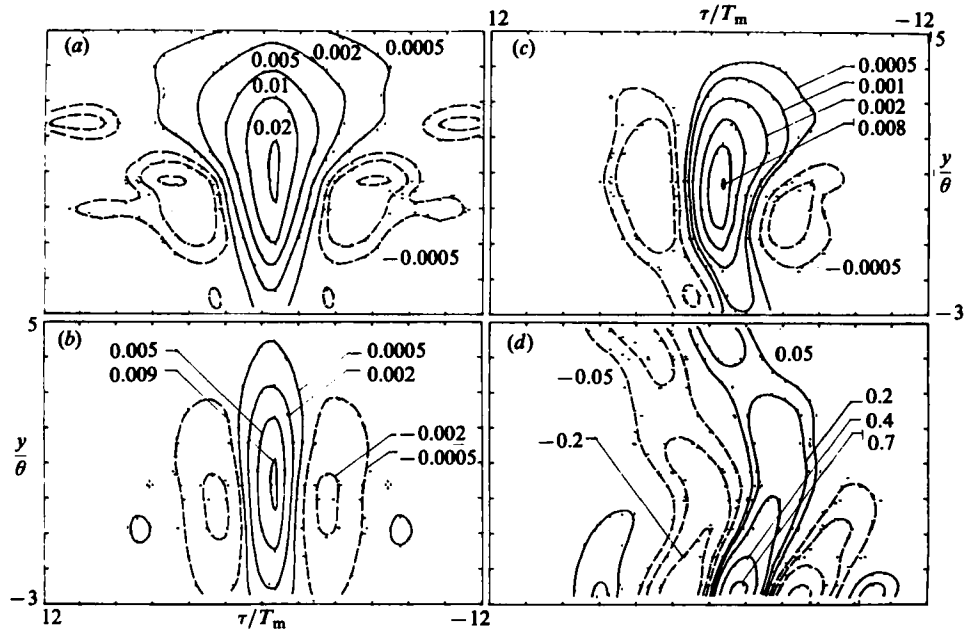

FIGURE 4. Contours of (*a*) $\overline{uu}(\tau)/U_e^2$; (*b*) $\overline{vv}(\tau)/U_e^2$; (*c*) $\overline{uv}(\tau)/U_e^2$; (*d*) $\overline{u_{r1}u}(\tau)/u'_{r1}u'$. Measurements at $x/\theta_e = 600$.

layer. The failure of this technique in the present flow could be partly due to hot-wire errors on the zero-speed side. However, although $\tilde{u}_{r2}$ obtained from the $U/U_e \approx 0.01$ point may be far from being the $\tilde{u}$-component of velocity there, it should be able to serve as a reference signal because the footprint of the large-scale structures should be clear in spite of hot-wire errors. (The successful eduction of the structure by triggering on the $\tilde{u}_{r2}$ peaks alone bears proof of this.) However, various combinations of (peaks and troughs of) $\tilde{u}_{r1}$ and $\tilde{u}_{r2}$ as joint criteria failed to capture even a semblance of pairing structures. Perhaps a much stricter criterion (thus requiring a prohibitively long experiment time) would be necessary to capture pairing structures. It is quite likely that not all structure interactions are of the complete pairing type in the high-Reynolds-number mixing layer. For comparison, note that the Reynolds number based on the maximum slope thickness at the last station in the present experiment was about 300000, as compared with 300 for Browand & Weidman's flow. Hussain & Clark (1981) suggested that with increasing Reynolds numbers the structure interactions involve not only complete pairing but also tearing and partial and fractional pairings. (It is also worth emphasizing that the single-stream mixing-layer behaviour has been found to be quite different from that of a two-stream mixing layer (Wygnanski *et al.* 1979; Browand & Latigo 1979; Hussain & Zedan 1978); space disallows a discussion here.)

In view of the foregoing, and previous results in ZH, the criterion of triggering on the positive peaks of $\tilde{u}_{r1}$, above the threshold level of 2σ (discussed in detail by ZH), has been used throughout the rest of this study; σ is the standard deviation of the a.c. coupled $\tilde{u}_{r1}$ signal. The smearing in the eduction by this technique was demonstrated to be insignificant by experiments in the axisymmetric mixing layer with and without excitation (see ZH and further discussion later).

3.3. *Coherent-structure properties*

3.3.1. *Structure passage frequency*

Figure 5(*a*) shows streamwise evolution of the power spectrum of u', measured on the high-speed edge of the mixing layer where $U/U_e \approx 0.99$. Note that the spectral peaks at 60 Hz and its harmonics are due to linearizer noise and are thus of no significance to the flow. The (linear) abscissa scales for these traces (as well as those in figure 5*b*) are indicated, but the (logarithmic) ordinate scales are arbitrarily chosen to highlight the spectral humps. It is remarkable that at each x-station the spectra traces exhibit an unambiguous hump. The distinct humps in the spectra not only indicate the presence of large-scale structures even when the layer originates from a fully turbulent initial condition, but also a quasiperiodicity in the passage of these structures everywhere in the flow. The hump frequency f_m decreases with increasing x, indicating the emergence of continually larger structures through interactions like pairing.

$\tilde{u}$-spectra for various locations across the mixing layer are shown in figure 5(*b*) for the streamwise station $x = 1200\theta_e$. It is apparent that the 'footprint' of the quasiperiodic structures is strongest near the high-speed edge of the mixing layer. Inside the mixing layer the hump is no longer noticeable in the spectrum owing to large-amplitude incoherent turbulence as well as to the fact that the coherent $\tilde{u}$-component is expected to be weak as the centre of the mixing layer is approached. A similar observation was made in the axisymmetric mixing layer by ZH and by others (e.g. Bradshaw, Ferris & Johnson 1964). The spectral hump reappears on the zero-speed side, but not as strongly as on the high-speed side. This should be partly due to the unavoidable hot-wire errors on the zero-speed side. It is also possible that the structure 'footprint' is relatively disorganized on this side. In the axisymmetric mixing layer (see ZH), the zero-speed side 'footprint' was found to be virtually non-existent as the spectrum showed no hump. Note that the hump frequency f_m on the zero-speed side is somewhat lower than that on the high-speed side. This is believed to be due to factors like tearing and pairings, which are also responsible for a large variation of f_m (as well as the convection velocity) across the axisymmetric mixing layer (Hussain & Clark 1981).

The second trace from the bottom in figure 5(*b*) was taken inside the potential flow on the high-speed side. The bottom trace was taken at the 99% velocity point in the boundary layer on the opposite wall parallel to the mixing layer (see figure 1). Disregarding the spectral peaks at 60 Hz and its harmonics associated with electronic noise (clearly visible in the largely amplified spectrum for the potential flow), no spurious spectral peaks are found in either of these two traces. This confirms that there is no dominant ambient disturbance or acoustic oscillation in the flow (note, for example, that Pui & Gartshore (1979) reported considerable difficulty in removing such disturbances), and that the quasiperiodic organized motion occurs only in the mixing layer. The bottom $\tilde{u}$-spectrum trace indicates that the boundary layer on the opposite wall is turbulent and is also devoid of any quasiperiodic motion. The absence of any common spectral peak for, say, the 99% velocity points of the mixing layer and the boundary layer on the opposite wall indicates that the transverse separation between the two is sufficient to preclude any coupling between the boundary-layer outer structure and the mixing-layer coherent structure, and that the mixing-layer organization is a feature unique to that layer.

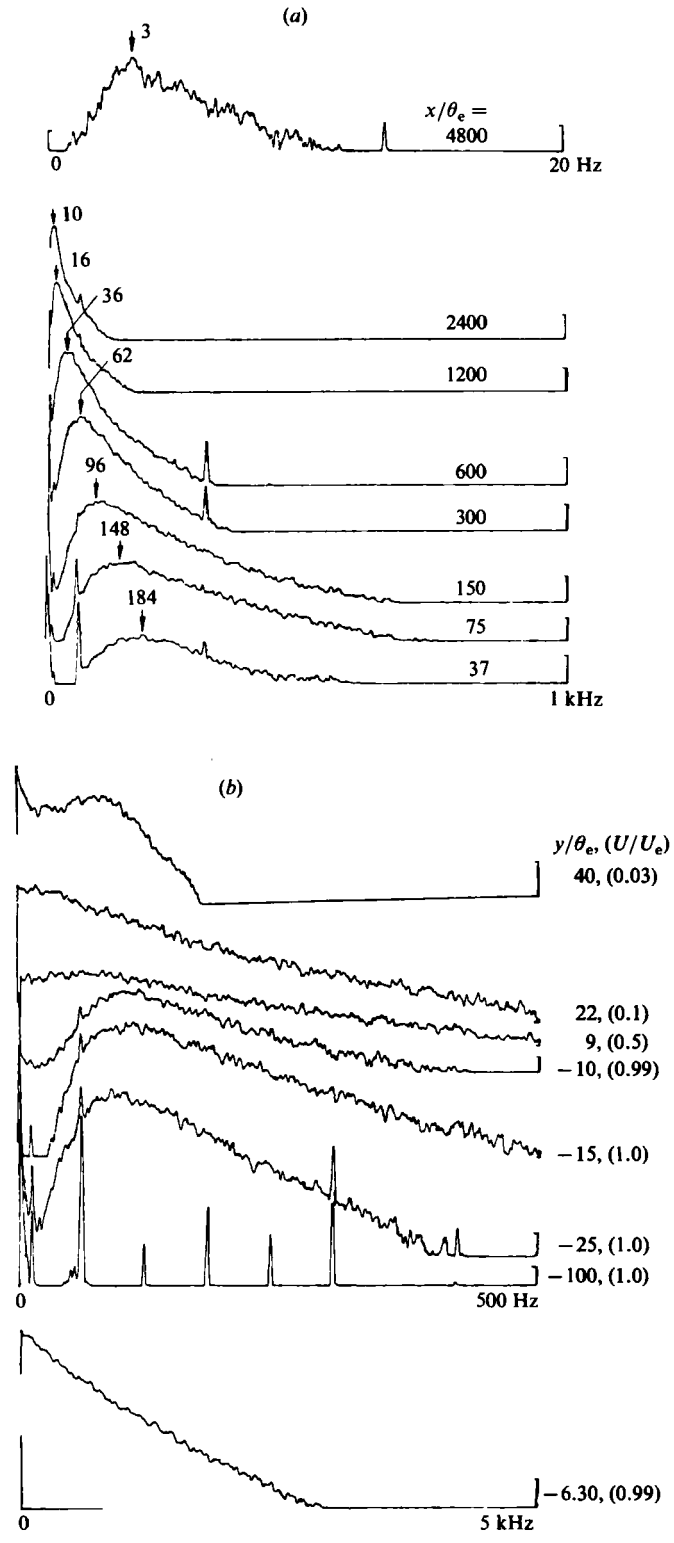

FIGURE 5. $\tilde{u}$-spectra: (*a*) for different x (all for the transverse location where $U/U_e \approx 0.99$); (*b*) for different transverse locations y (all for $x/\theta_e = 1200$).

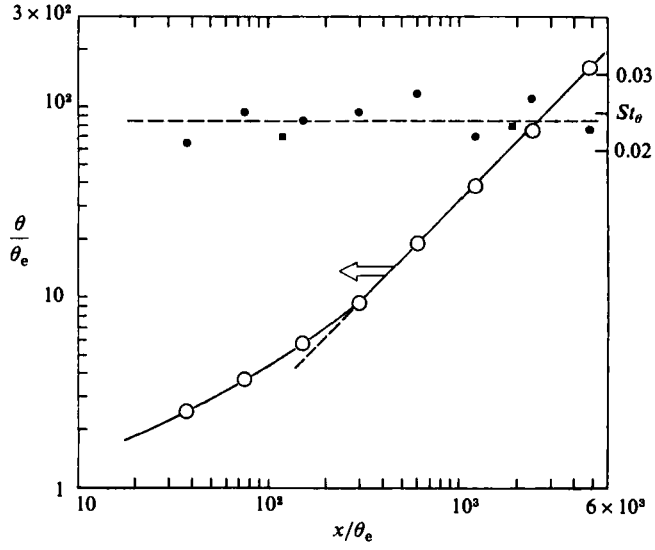

FIGURE 6. Streamwise variation of local momentum thickness θ (○), and Strouhal number $St_\theta = f_m\theta/U_e$ (● for $U_e = 12$ m s^{-1}, ■ for $U_e = 9$ m s^{-1}).

The similarity scaling of the dominant frequency f_m is demonstrated in figure 6, which also shows the streamwise evolution of the local momentum thickness

$$\theta = \int_{y_{0.1}}^{\infty} \frac{U}{U_e}\left(1-\frac{U}{U_e}\right) \mathrm{d}y.$$

Note that, in order to eliminate the effects of hot-wire errors on the zero-speed side, the profile integration has been terminated at the transverse location $y_{0.1}$ where $U/U_e \approx 0.1$. This truncation would underestimate θ (by exactly 10% for the tanh profile); however, there is an error in the measurement of U due to high turbulence (including flow reversal), producing an overestimate of θ; thus the two errors should have a cancelling effect, and the measured θ should be a good approximation of the actual θ. Figure 6 shows that θ increases linearly with x for $x \gtrsim 300\theta_e$, and $\mathrm{d}\theta/\mathrm{d}x$ increases progressively with increasing x from the origin to $x \approx 300\theta_e$. This location for achievement of self-preservation was also found by previous investigators (Foss 1977; Hussain & Zedan 1978), who also noted a lower slope of $\theta(x)$ for $x \lesssim 300\theta_e$. Hussain & Zedan further showed that this length for achievement of self-preservation decreases somewhat with increasing values of the initial momentum-thickness Reynolds number R_θ, and that, if u' profiles are considered, self-preservation occurs further downstream, i.e. beyond $x \approx 500\theta_e$. The asymptotic spread rate $\mathrm{d}\theta/\mathrm{d}x$ in figure 6 is 0.032, which is in agreement with the values reported by Hussain & Zedan (1978) and others for initially tripped mixing layers. Note that since $\mathrm{d}\theta/\mathrm{d}x$ equals V_E/U_e (where V_E is the transverse entrainment velocity on the zero-speed side), the above data give a measurement of the entrainment velocity V_E, which is thus 3.2% of the free-stream velocity U_e.

When the average structure passage frequency f_m, inferred from the spectral hump (figure 5*a*), is used to form a *local Strouhal number* St_θ ($= f_m\theta/U_e$), it is found to be a *constant* (≈ 0.024) for the entire x-range of measurement (figure 6). Since θ increases linearly with x, f_m ($\approx 0.024U_e/\theta$) is inversely proportional to x. Note that if one takes the average time period in the oscillations of the autocorrelation data

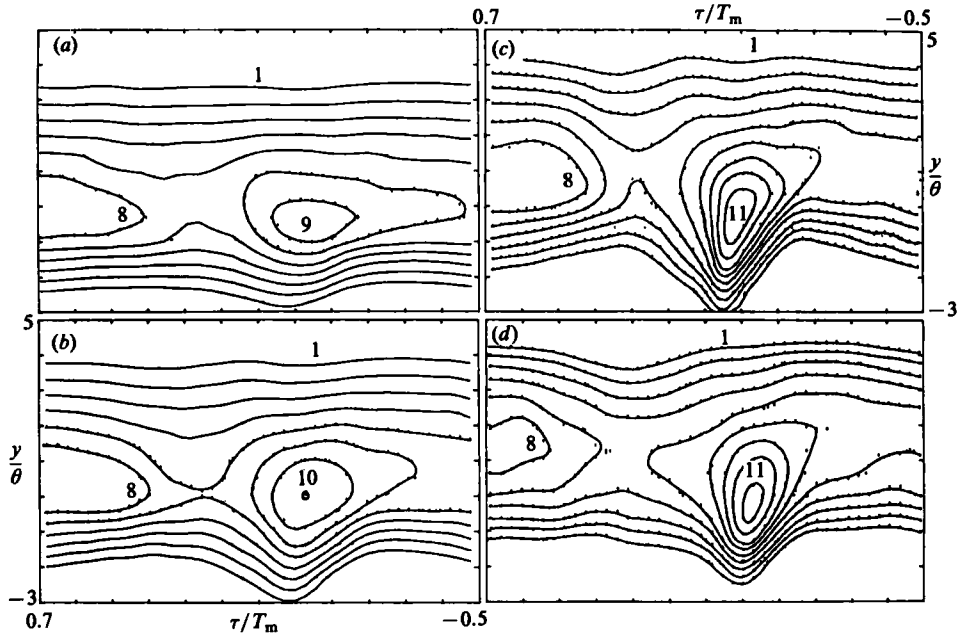

FIGURE 7. Ω_z/f_m contours for: (*a*) $x = 150\theta_e$; (*b*) $300\theta_e$; (*c*) $600\theta_e$; (*d*) $4800\theta_e$. Successive contours are at an increment of 1.

of Dimotakis & Brown (1976), measured in a two-stream mixing layer, and estimates the value of St_θ, a comparable value is obtained. The scatter in the data in figure 6 is primarily due to the uncertainty in the measurement of f_m.

3.3.2. *The equilibrium structure properties*

Figures 7 (*a–d*) show the contours of coherent spanwise vorticity at different stages of evolution of the structure, namely at $x/\theta_e = 150$, 300, 600 and 4800. The last station corresponds to a Reynolds number $R_x \approx 2 \times 10^6$. Contours of vorticity and various other properties have also been obtained at $x \approx 2000\theta_e$, but are not presented because the details are between those at $x/\theta_e = 600$ and $x/\theta_e = 4800$, which themselves are quite similar within the experimental uncertainty. Note that the contours are plotted as a function of the transverse distance (non-dimensionalized by the local lengthscale θ) and the time (non-dimensionalized by the local average passage time $T_m = 1/f_m$, where $f_m \theta/U_e = 0.024$). The time τ is measured from the instant of trigger (i.e. the occurrence of $\tilde{u}$-peaks on the high-speed edge of the mixing layer). No attempt was made to capture the earlier stages of the roll-up process ($x < 150\theta_e$) because of the poorer spatial resolution in the thin layer and the finite size of the X-wire.

The roll-up of the initially turbulent mixing layer first results in a relatively elongated structure. Even though the actual structure size (especially its length) increases from $x/\theta_e \approx 150$ to 300, the aspect ratio decreases because the roll-up process starts first with an elongated structure cross-section, which progressively becomes more rounded. This is consistent with visualization pictures (see e.g. Fiedler *et al.* 1980). Note that, even though the structure shape changes significantly between $x = 150\theta_e$ and $300\theta_e$, the change in the non-dimensional vorticity is not drastic. The roll-up is complete soon after $x/\theta_e = 300$, after which the contours achieve a

self-preserving state. A similar roll-up process was also observed in an initially turbulent axisymmetric mixing layer (Hussain & Zaman 1981*a*, *hereinafter referred to as* HZ2) and a plane mixing layer (Oster *et al.* 1977), both subjected to controlled excitation. Note that the abscissa scale in figure 7 is so chosen that the spatial extent of the structures, assuming a convection velocity of $0.5U_e$, is compressed in the streamwise direction (relative to the transverse direction) by a factor of two at all stations.

The essentially similar coherent vorticity-contour details at $x/\theta_e = 600$, 2000 (not shown) and 4800 suggest achievement of an 'equilibrium' state which persists for the entire length of plane mixing layer. (The actual structure dimension increases linearly and the dimensional peak coherent vorticity decreases linearly with increasing x in the self-preserving region.) Note that contours at $x/\theta_e = 4800$ suggest a slightly increased smearing in comparison with those at $x/\theta_e = 600$. While this might arise from slightly increased variability and transverse wandering of the structures or even measurement errors due to the significantly increased experiment time at $x/\theta_e = 4800$, the differences between the two self-preserving structures at $x/\theta_e = 600$ and 4800 are within the experimental uncertainty.

The eduction captures part of a repeated structure on the left of each figure due to the quasiperiodicity in the structure passage. However, this repeated part is significantly smeared – an effect that increases with increasing time (or distance) away from the trigger (see ZH); note that $\tau = 0$ represents the triggering instant.

It is necessary to emphasize that the smearing in the structure core introduced by the eduction process is not significant. The extent of smearing had been evaluated in the axisymmetric mixing layer (see ZH) by comparing the natural structure, educed by applying the same conditional-sampling technique as used here, with the structure induced (and made periodic) via small-amplitude excitation at the preferred mode. In the excited flow the structure details were known accurately by independent, phase-locked measurements which involved minimal smearing (see HZ2). That the smearing was minimal was evident from an essentially identical repeated structure educed one wavelength apart. This phase-averaged structure in the excited flow agreed quite well in shape, size, peak vorticity level, etc. with the natural structure. (For further details see ZH, which also reports the sensitivity of the structures to the excitation amplitude.) This therefore provides an adequate validation of the eduction scheme and proof that there is indeed negligible smearing at the structure core. It is worthwhile to mention that other researchers (e.g. P. E. Dimotakis, private communication) had suggested that the peak values in our coherent-vorticity data must be significantly smeared out, perhaps by an order of magnitude, as a result of the ensemble averaging. The above discussion should convince one that this cannot be true.

Figures 8(*a–d*) show the contours of incoherent Reynolds stress $\langle u_r v_r \rangle / U_e^2$ for the four x-stations of figure 7. In these and subsequent figures, the + symbol denotes the location of the peak vorticity inferred from figures 7(*a–d*). The roll-up process organizes the fine-grained turbulence into longitudinally separated patches of $\langle u_r v_r \rangle$. It is clear that the peak vorticity, which also corresponds to the location of maximum rate of change in vorticity, occurs at the 'minimax' of the $\langle u_r v_r \rangle$ distribution (HZ1). With increased organization of the incoherent turbulence by the coherent structure, the $\langle u_r v_r \rangle$ contour is progressively 'kinked' until the self-preserving shape is reached. Since incoherent turbulence data can be viewed as independent of the vorticity measurements, the essentially similar $\langle u_r v_r \rangle$ contours at the last two stations – which are $4200\theta_e$ apart – further confirm the achievement of an 'equilibrium state' of the

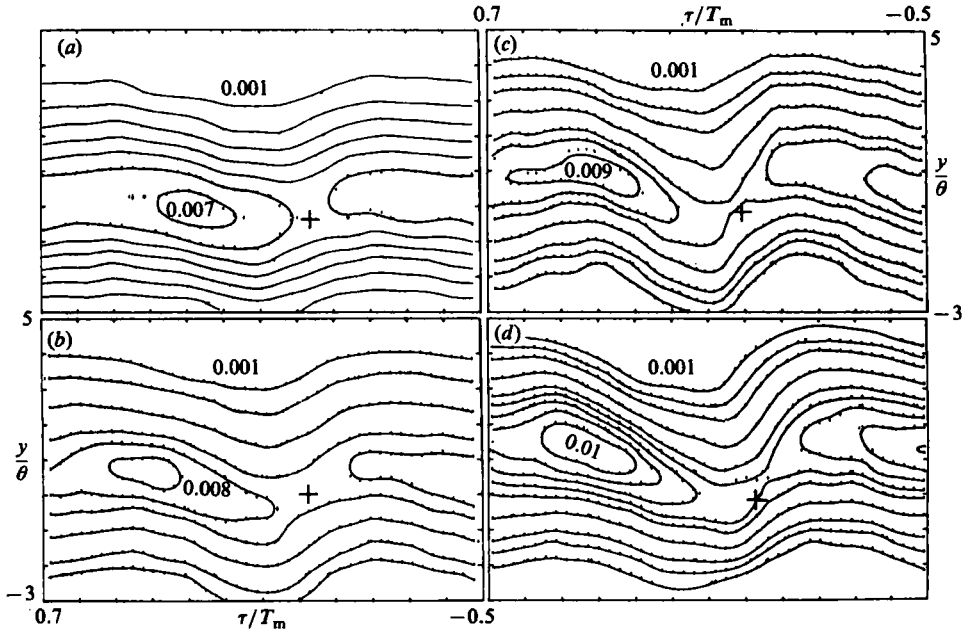

FIGURE 8. Contours of $\langle u_r v_r \rangle / U_e^2$ for the four stations of figure 7. Unmarked contour levels are (*a*) ($x/\theta_e = 150$) 0.002, 0.003, 0.004, 0.005, 0.006; (*b*) ($x/\theta_e = 300$) 0.002, 0.004, 0.006, 0.007; (*c*) ($x/\theta_e = 600$) 0.002, 0.003, 0.005, 0.007, 0.008; (*d*) ($x/\theta_e = 4800$) 0.002, 0.003, 0.005, 0.007, 0.008, 0.009.

coherent structure. It is interesting to note that the (non-dimensional) transverse extents of Ω_z and $\langle u_r v_r \rangle$ contours are the same at different x. Hence the growth of the time-average width of the mixing layer is not a mere consequence of increased lateral wandering of the structures. The individual structures must also be increasing in size with increasing x at the same rate as the time-average thickness.

Figures 9(*a–d*) show the contours of the coherent Reynolds stress $\langle u_p v_p \rangle / U_e^2$ at $x/\theta_e = 150$, 300, 600 and 4800. As the initially turbulent layer rolls up into rounded structures, $\langle u_p v_p \rangle$ increases from the initial zero value at a much faster rate than $\langle u_r v_r \rangle$, and reaches the asymptotic state for $x/\theta_e \lesssim 600$. The evolution of the $\langle u_p v_p \rangle$ distribution in the present study differs in many ways from that in the axisymmetric mixing layer. In an initially laminar axisymmetric mixing layer under controlled excitation (see HZ1), the highly organized laminar vortices produce large $\langle u_p v_p \rangle$ but zero $\langle u_r v_r \rangle$. As the vortices undergo transition downstream, $\langle u_p v_p \rangle$ peak values drop but $\langle u_r v_r \rangle$ peak values increase, the two becoming comparable at the end of the potential core. Also, the $\langle u_p v_p \rangle$ values are found to be very small on the zero-speed side of the axisymmetric mixing layer (see also HZ2), in contrast with the equal extents of the $\langle u_p v_p \rangle$ contours on either side of the plane mixing layer. This is attributable to the dilation of the structure footprint on the zero-speed side in the axisymmetric case. Furthermore, in the two studies of the axisymmetric mixing layer under controlled excitation (cited above), positive and negative contours of $\langle u_p v_p \rangle$ occurred alternately in x owing to the periodic passage of the induced structures. This is not the case in the present study because the natural structures are less periodic and jitter increases with increasing time away from the trigger.

Thus $\langle u_p v_p \rangle$ contours in the present study are expected to have regions of positive and negative values only around the structure centre in a 'cloverleaf' fashion

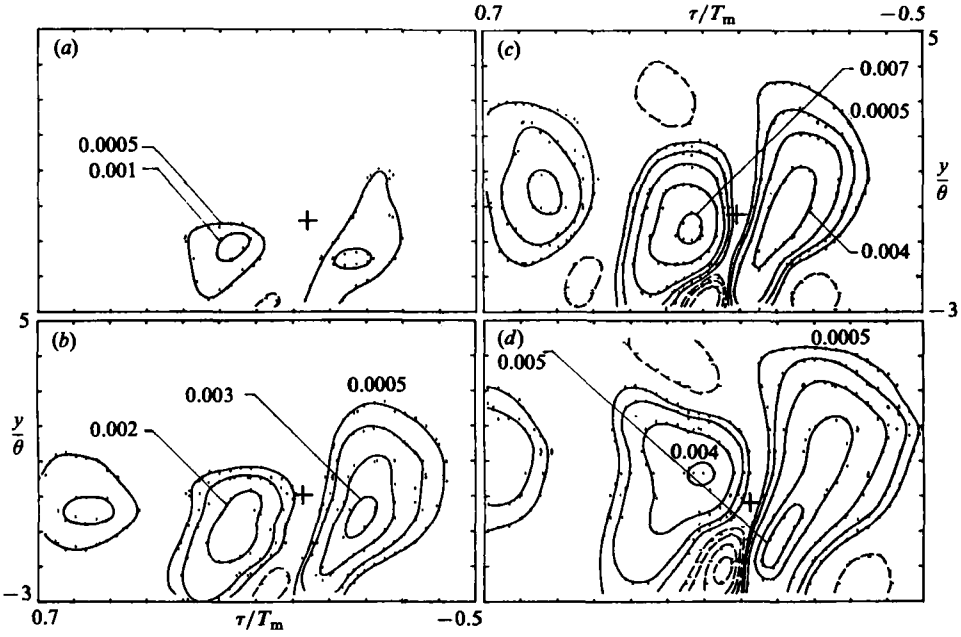

FIGURE 9. Contours of $\langle u_p v_p \rangle / U_e^2$ for the four stations of figure 7. Contour levels are (*a*) ($x/\theta_e = 150$) ± 0.0005, 0.001; (*b*) ($x/\theta_e = 300$) ± 0.0005, 0.001, 0.002, 0.003; (*c*) ($x/\theta_e = 600$) ± 0.0005, ± 0.001, ± 0.002, 0.004, 0.007; (*d*) ($x/\theta_e = 4800$) ± 0.0005, ± 0.001, ± 0.002, ± 0.003, 0.004, 0.005.

(figure 9), the positive values being of the cogradient type and the negative values being of the countergradient type. Note that the contours at $x/\theta_e = 600$ and 4800 are quite similar, considering the fact that $\langle u_p v_p \rangle$ is expected to have a large uncertainty. In particular, the orientations of the four regions of the 'cloverleaf' arrangement are indeed very similar at the last two stations. Note also that the peak values of $\langle u_p v_p \rangle$ do not exceed the time-average value $\overline{uv}$, and are comparable to the peak values of $\langle u_r v_r \rangle$. This indicates that both coherent and incoherent motions are significant in contributing to the Reynolds stress.

The relative extents of the areas of positive and negative $\langle u_p v_p \rangle$ contours should depend on the orientation of the structure. Consider a coherent structure in a shear layer for three configurations identified by the streamlines in figure 10. The corresponding contours of $\langle u_p v_p \rangle$ are schematically indicated by the hatched regions. The association of the four regions of $\langle u_p v_p \rangle$ with the structure is a straightforward consequence of the streamline shape in a frame advected with the structure centre (also emphasized by F. K. Browand at the 1980 APS meeting). It is clear from figure 9 that the measured $\langle u_p v_p \rangle$ distribution is similar to that in figure 10(*c*), the cogradient contributions significantly exceeding the countergradient contributions. In this case the time-average Reynolds stress will be of the cogradient type. However, if the structures pass by with an orientation as in figure 10(*b*) (say under controlled excitation), countergradient Reynolds stress and hence the so-called 'negative production' will occur. Such countergradient Reynolds stress has also been observed to occur at a certain stage of vortex pairing, when the pairing process is phase-locked in space by controlled excitation (HZ1); that is, this stage of pairing, which produces countergradient $\langle u_p v_p \rangle$, is forced by the controlled excitation to occur periodically at the same spatial location. The (time-average) Reynolds stress

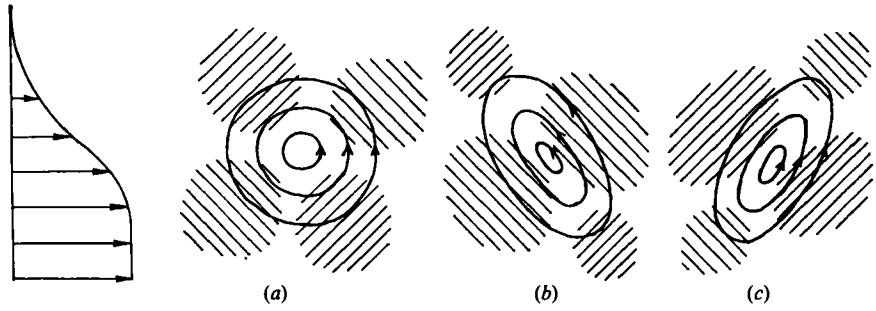

FIGURE 10. Schematic of a coherent structure in three different orientations and associated regions (shown by hatched lines) of coherent Reynolds stress $\langle u_p v_p \rangle$: ▨, positive $\langle u_p v_p \rangle$; ▩, negative $\langle u_p v_p \rangle$.

and production in this flow were indeed found to be negative in a large region associated with this stage of pairing (see HZ1). The results of Oster & Wygnanski (1982) showing negative production without pairing should imply that the periodic excitation in their experiment forced the single structures with the countergradient orientation to occur at the corresponding measurement location.

Further details of the 'equilibrium' coherent structure are shown in figure 11. For the $x = 4800\theta_e$ station, contours of $\langle u_p \rangle / U_e$, $\langle v_p \rangle / U_e$ and $\langle u_r^2 \rangle^{\frac{1}{2}} / U_e$ are shown in figures 11 (a, b, c) respectively. Figure 11 (d) shows the coherent shear production

$$-\langle P_s \rangle = \frac{\langle u_r v_r \rangle}{f_m U_e^2} \left[\frac{\partial \langle u \rangle}{\partial y} - \frac{1}{0.5 U_e} \frac{\partial \langle v \rangle}{\partial t} \right].$$

The $\langle u_p \rangle$ and $\langle v_p \rangle$ contours suggest a structure orientation on the high-speed side similar to that in figure 10(c), although the educed structure shape (see figure 7d) is not as simple, especially on the zero-speed side. The peak values of $\langle u_p \rangle$ and $\langle v_p \rangle$ are both about 10% of the free-stream velocity. The corresponding peak values in the axisymmetric mixing layers were found to be somewhat higher in the unexcited case (ZH) and considerably higher in the excitation case (HZ2). Comparison of the $\langle u_p \rangle$ and Ω_z contours (figures 11a, 7d) show that $\langle u_p \rangle$ contours are not useful for identification of the structure boundary (see also HZ1). Thus the success of $\langle u_p \rangle$ contours in the identification of the 'spot' boundary is unique to the boundary layer (Wygnanski, Sokolov & Friedman 1976; Cantwell, Coles & Dimotakis 1978), and should not be expected in general.

$\langle u_r^2 \rangle^{\frac{1}{2}}$ distribution (figure 11c) shows a peak near the structure centre, somewhat similar to the corresponding data in the axisymmetric mixing layer under controlled excitation (HZ2). Note that the $\langle u_r^2 \rangle^{\frac{1}{2}}$ peak at the repeated structure centre away from the trigger occupies a larger area (on the left as well as on the right of figure 11c). This is due to increasing jitter with increasing time away from the trigger, as discussed earlier.

The contours of coherent shear production $\langle P_s \rangle$ (figure 11d) reveal that most production occurs in the braid (i.e. the 'saddle'); production in the structure core (i.e. the 'centre') is negligible. Thus the saddle is the dynamically most important part of the coherent structure. Measurements of normal production

$$\langle P_n \rangle = -\langle u_r^2 \rangle \frac{\partial \langle u_p \rangle}{\partial x} - \langle v_r^2 \rangle \frac{\partial \langle v_p \rangle}{\partial y}$$

show that it is considerably smaller than $\langle P_s \rangle$. Hence $\langle P_s \rangle \approx \langle P \rangle$ in the selected

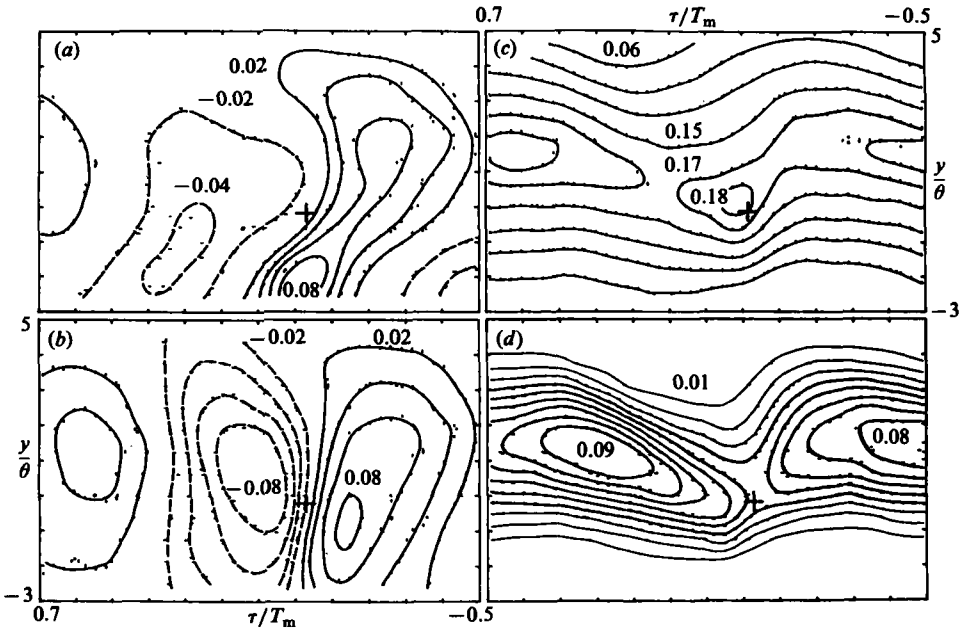

FIGURE 11. Contours of different properties measured at $x/\theta_e = 4800$: (*a*) $\langle u_p \rangle / U_e$, contour levels are ± 0.02, ± 0.04, 0.06, 0.08; (*b*) $\langle v_p \rangle / U_e$, same levels as in (*a*); (*c*) $\langle u_r^2 \rangle^{\frac{1}{2}} / U_e$, contour levels are 0.06, 0.09, 0.12, 0.15, 0.17, 0.18; (*d*) $-\langle P_s \rangle$, successive contour levels are at the increment of 0.01.

coordinates; note that $\langle P \rangle = \langle P_s \rangle + \langle P_n \rangle$. Since it is $\langle P \rangle$ that is invariant under coordinate rotation, and neither $\langle P_s \rangle$ nor $\langle P_n \rangle$ is, the discussion is more rigorous when made in terms of $\langle P \rangle$. The $\langle P \rangle$ contours here are very similar to those in the axisymmetric mixing layer (Hussain 1980). Note that the peak value of $\langle P \rangle$ is found to be only about 50% higher than the peak value of time-average production $\overline{P} = -\overline{uv}(\partial U/\partial y + \partial V/\partial x)$.

Based on our extensive quantitative and visualization studies of coherent structures, it was argued by Hussain (1983) that production in the braid must involve longitudinal vortices, called 'ribs', whose continual stretching by the rolls must be the central mechanism for turbulence production (see also Coles 1983; Neu 1984). The low spanwise vorticity measured in the braid (figure 7) is consistent with the existence of ribs. The so-called large-scale spanwise rolls are thus connected by longitudinal rib vortices. The ribs must obviously turn and connect to each other within the rolls. Hence, even though the rolls are two-dimensional on an ensemble-average basis (see also Browand & Troutt 1980; Breidenthal, private communication), they must be strongly three-dimensional instantaneously. Three-dimensional time-dependent numerical simulation (R. W. Metcalfe, private communication), and flow visualization by us and others (Bernal 1981; Smith 1983; Katz, private communication) have also revealed longitudinal vortices in the braid.

Thus the rolls are connected to each other via longitudinal vortices, namely ribs. The rotation of the rolls produces longitudinal stretching of the ribs. This therefore is the central mechanism for turbulence production. Turbulence produced via this vortex stretching is advected away from the braid by the rotational motion of the structures and deposited to the structure core. Thus the coherent structures carry with them the mechanism of their sustenance. The ribs are transversely displaced with

respect to each other, making the braid a 'perforated' sheet; that is, fluid can cross the mixing layer across the braid without being entrained. The longitudinal stretching of a rib along its axis (the diverging separatrix) results in 'production' via spinning. This enhances velocity fluctuations normal to the diverging separatrix, but is not central to mixing. When this spinning fluid with vorticity predominantly along the diverging separatrix reaches the rolls with predominantly spanwise vorticity, the interaction of the orthogonal vorticities produces three-dimensional vorticity fluctuations and hence true mixing or entrainment. For a discussion of further details and implications of these concepts see Hussain (1983).

The mechanism for the formation of the ribs in the braid is unknown, but is perhaps related to Taylor–Görtler-type instability of the braid. Continued efforts are underway in our laboratory to unravel further topological details of coherent structures in mixing layers, jets, wakes, boundary layers and pipe flows.

4. Concluding remarks

In this study we have addressed the nature of organization of a large, single-stream, unexcited plane mixing layer originating from a *fully developed turbulent boundary layer*. Care was exercised to assure that the flow was free from any noticeable oscillation otherwise associated with flow pulsations or acoustic modes and that there was no coupling between the mixing layer and the outer structures of the boundary layers on the confining walls. Appropriate tripping was used so that the exit boundary layer initiating the shear layer agreed well with the equilibrium flat-plate turbulent boundary layer. This initially fully turbulent shear layer rolls up into periodic organized structures. From the spectrum of the longitudinal velocity signal derived from the high-speed edge of the mixing layer, the passage of large-scale structures is detectable as clear spectral humps everywhere along the length of the mixing layer. The frequency f_m of this hump, denoting the average structure passage frequency, decreases progressively with increasing x. Based on the local shear-layer momentum thickness θ, the Strouhal number $f_m\theta/U_e$ has a constant value of about 0.024. Since θ increases linearly with x in the self-preserving region, $f_m x/U_e$ is also (≈ 0.75) in this region. The self-preserving region occurs for $x/\theta_e \gtrsim 500$, where the large-scale structures achieve an 'equilibrium state'. This location for achievement of self-preservation is consistent with time-average measures like $\theta(x)$. From $\mathrm{d}\theta/\mathrm{d}x$ it is inferred that the zero-speed side entrainment velocity for a single-stream plane mixing layer is 3.2% of the free-stream velocity.

The simple, conditional-sampling technique of triggering on the positive peaks of a reference $\tilde{u}$-signal (above a threshold of 2σ) obtained from the high-speed edge of the mixing layer has been found to be adequate for educing the large-scale structures. Stricter criteria using the positive and negative peaks of reference $\tilde{u}$-signals obtained from the high- and zero-speed sides of the mixing layer did not prove to be significantly better. In particular, joint eduction criteria based on the high- and zero-speed-side reference signals did neither significantly improve the eduction nor capture structures during interaction. The two-signal detection scheme was successfully used by Browand & Weidman (1976) for eduction of a pairing phase of the structures, in a much lower-Reynolds number flow. This would suggest that, while structure interaction is of the complete pairing type at low Reynolds numbers, other modes of interaction, like tearing and partial and fractional pairings, may occur at higher Reynolds numbers (Hussain & Clark 1981). The educed structure is therefore the average dominant structure, even though individual structures would vary in

shape, size, orientation, strength, convection velocity, etc. The eduction scheme sifts out only the strongest structures. In this sense, the educed structure is a select, albeit dominant, structure.

A question that naturally arises is: to what extent are the educed properties smeared out by ensemble averaging implicit in the eduction process? Ensemble averaging is necessary so that individual peculiarities are deemphasized. It also helps in the spatial smoothing necessary to eliminate the internal fluctuations associated with incoherent turbulence. However, the threshold criterion selects a subclass of similar structures so that smearing is not likely to be significant. The insignificant smearing in the vicinity of the trigger location was demonstrated in the axisymmetric mixing layer by the application of a small-amplitude excitation (ZH). The excitation made the large-scale structures periodic; thus the educed structure in this flow suffered least from smearing. Yet the educed Ω_z contours in this flow agreed well with the Ω_z contours educed in the unexcited case. Thus, although the smearing is large in the natural case in regions far away from the trigger, e.g. in the repeated structure one wavelength away, it should not be significant in the core of the structure near the trigger.

The educed contour properties are helpful provided that the structures are globally two-dimensional. Previous investigations have claimed that the large-scale structures are basically two-dimensional (Wygnanski *et al.* 1979; Browand & Troutt 1980). Spanwise correlation measurements in our facility also revealed two-dimensionality on the average (S. J. Kleis, private communication), even though the structures ought to consist of highly three-dimensional internal substructures.

The detailed contour properties like coherent vorticity, Reynolds stress, and production and incoherent Reynolds stress and intensities during the evolving and asymptotic states have been documented. Both the structure properties and the relative successes of the eduction schemes have been examined in comparison with those in the axisymmetric mixing layer. The structures have a stronger transverse coherence in the plane layer in comparison with that in the axisymmetric layer; consequently, the zero-speed side 'footprint' in the plane layer is comparatively stronger.

We appreciate financial support from NASA Ames Research Center under grant NSG-2337 and discussions with Joe Marvin and John Viegas.

REFERENCES

Antonia, R., Chambers, A. J. & Hussain, A. K. M. F. 1980 *Phys. Fluids* **23**, 871.

Bernal, L. 1981 Ph.D. thesis, California Institute of Technology.

Batt, R. G. 1975 *AIAA J.* **13**, 245.

Bradshaw, P. 1966 *J. Fluid Mech.* **26**, 225.

Bradshaw, P., Ferris, D. H. & Johnson, R. H. 1964 *J. Fluid Mech.* **19**, 591.

Browand, F. K. & Latigo, B. O. 1979 *Phys. Fluids* **22**, 1011.

Browand, F. K. & Troutt, T. R. 1980 *J. Fluid Mech.* **97**, 771.

Browand, F. K. & Weidman, P. D. 1976 *J. Fluid Mech.* **76**, 127.

Brown, G. L. & Roshko, A. 1974 *J. Fluid Mech.* **64**, 775.

Brown, G. L. & Thomas, A. S. W. 1977 *Phys. Fluids Suppl.* **20**, S243.

Cantwell, B., Coles, D. & Dimotakis, P. E. 1978 *J. Fluid Mech.* **87**, 641.

Cimbala, J. M. 1984 Ph.D. thesis, California Institute of Technology.

COLES, D. E. 1962 *Rand Corp. Rep.* R-403-PR.

COLES, D. 1983 In *Turbulence and Chaotic Phenomena in Fluids* (ed. T. Tatsumi), p. 397. North-Holland.

CROW, S. C. & CHAMPAGNE, F. H. 1971 *J. Fluid Mech.* **48**, 547.

DIMOTAKIS, P. E. & BROWN, G. L. 1976 *J. Fluid Mech.* **78**, 535.

FIEDLER, H. E., DZIOMBA, B., MENSING, P. & RÖSGEN, T. 1980 In *Role of Coherent Structures in Modelling Turbulence and Mixing* (ed. J. Jimenez), Lecture Notes in Physics, vol 136, p. 219. Springer.

FOSS, J. F. 1977 *Turb. Shear Flows, Penn. State Univ.* 11.33.

GRANT, H. L. 1958 *J. Fluid Mech.* **4**, 149.

HEAD, M. R. & BANDYOPADHYAY, P. 1981 *J. Fluid Mech.* **107**, 297.

HUSSAIN, A. K. M. F. 1980 In *Role of Coherent Structures in Modelling Turbulence and Mixing* (ed. J. Jimenez), Lecture Notes in Physics, vol. 136, p. 252. Springer.

HUSSAIN, A. K. M. F. 1980 In Lecture Notes in Physics (ed. J. Jimenez), vol. 136, p. 252.

HUSSAIN, A. K. M. F. 1983 In *Turbulence and Chaotic Phenomena in Fluids* (ed. T. Tatsumi), p. 453. North-Holland.

HUSSAIN, A. K. M. F. & CLARK, A. R. 1981 *J. Fluid Mech.* **104**, 263.

HUSSAIN, A. K. M. F. & ZAMAN, K. B. M. Q. 1980 *J. Fluid Mech.* **101**, 493.

HUSSAIN, A. K. M. F. & ZAMAN, K. B. M. Q. 1981*a* *J. Fluid Mech.* **110**, 39.

HUSSAIN, A. K. M. F. & ZAMAN, K. B. M. Q. 1981*b* *Bull. Am. Phys. Soc.* **26**, 1251.

HUSSAIN, A. K. M. F. & ZAMAN, K. B. M. Q. 1982 *Rep.* FR-14, *Aerodyn. & Turbulence Lab., Univ. Houston.*

HUSSAIN, A. K. M. F. & ZEDAN, M. F. 1978 *Phys. Fluids* **21**, 1100.

KEFFER, J. F. 1965 *J. Fluid Mech.* **22**, 135.

MOALLEMI, M. K. & GOLDSCHMIDT, V. W. 1981 *Purdue Univ. Rep.* HL 81–82.

MUMFORD, J. C. 1982 *J. Fluid Mech.* (to appear).

NEU, J. C. 1984 *J. Fluid Mech.* **143**, 253.

OSTER, D. & WYGNANSKI, I. 1982 *J. Fluid Mech.* **123**, 91.

OSTER, D., WYGNANSKI, I., DZIOMBA, B. & FIEDLER, H. 1977 In *Structure and Mechanisms of Turbulence I* (ed. H. Fiedler). Lecture Notes in Physics, vol. 75, p. 48. Springer.

PUI, N. K. & GARTSHORE, I. S. 1979 *J. Fluid Mech.* **91**, 111.

PURTELL, L. P., KLEBANOFF, P. S. & BUCKLEY, F. T. 1981 *Phys. Fluids* **24**, 802.

ROSHKO, A. 1980 In *Role of Coherent Structures in Modelling Turbulence and Mixing* (ed. J. Jimenez), Lecture Notes in Physics, vol. 136, p. 208. Springer.

SMITH, C. R. 1983 *Turbulence Symp., Rolla*, vol. 8, p. 299.

TOWNSEND, A. A. 1979 *J. Fluid Mech.* **95**, 515.

TSO, J. 1983 Ph.D. thesis, Johns Hopkins University.

WYGNANSKI, I., OSTER, D., FIEDLER, H. & DZIOMBA, B. 1979 *J. Fluid Mech.* **93**, 325.

WYGNANSKI, I., SOKOLOV, M. & FRIEDMAN, D. 1976 *J. Fluid Mech.* **78**, 785.

YULE, A. J. 1978 *J. Fluid Mech.* **89**, 413.

ZAMAN, K. B. M. Q. & HUSSAIN, A. K. M. F. 1981 *J. Fluid Mech.* **112**, 379.

ZAMAN, K. B. M. Q. & HUSSAIN, A. K. M. F. 1984 *J. Fluid Mech.* **138**, 325.